Effect of Co-Solvents on the Crystallization and Phase Distribution of Mixed-Dimensional Perovskites

Wiley Analytical Science

Wiley Analytical Science Virtual Conference

November 9-17

For the 3rd time, The Wiley Analytical Science Conference is back!

It's all happening November 9 - 17

The Wiley Analytical Science Virtual Conference will bring together thousands of researchers and practitioners to share current developments in science and industry. Join for exciting presentations from experts in the fields of analytical and bioanalytical chemistry, pharmaceutical research, materials science, lab automation, and related disciplines.

Register to learn about recent developments & applications in:

- Microscopy
- Spectroscopy
- Mass Spectrometry
- Separation Science
- Much more!

Register here

WILEY

ADVANCED ENERGY MATERIALS
www.advenergymat.de

Effect of Co-Solvents on the Crystallization and Phase Distribution of Mixed-Dimensional Perovskites

*Alessandro Caiazzo, Kunal Datta, Junke Jiang, María C. Gélvez-Rueda, Junyu Li, Riccardo Ollearo, José Manuel Vicent-Luna, Shuxia Tao, Ferdinand C. Grozema, Martijn M. Wienk, and René A. J. Janssen**

Solution-processed quasi-2D perovskites are promising for stable and efficient solar cells because of their superior environmental stability compared to 3D perovskites and tunable optoelectronic properties. Changing the number of inorganic layers (*n*) sandwiched between the organic spacers allows for tuning of the bandgap. However, narrowing the phase distribution around a specific *n*-value is a challenge. In-situ UV–vis–NIR absorption spectroscopy is used to time-resolve the crystallization dynamics of quasi-2D butylammonium-based (BA) perovskites with <*n*> = 4, processed from *N*,*N*-dimethylformamide (DMF) in the presence of different co-solvents. By combining with photoluminescence, transient absorption, and grazing-incidence wide-angle X-ray scattering, the crystallization is correlated to the distribution of phases with different *n*-values. Infrared spectroscopy and density functional theory reveal that the phase distribution correlates with perovskite precursor—co-solvent interaction energies and that stronger interactions shift the phase distribution towards smaller *n*-values. Careful tuning of the solvent/co-solvent ratio provides a more homogeneous phase distribution, with highly oriented perovskite crystals and suppressed formation of *n* = 1–2 phases, providing a power conversion efficiency for $BA_2MA_3Pb_4I_{13}$ solar cells that increases from 3.5% when processed from DMF to over 11% and 10% when processed from DMF/dimethyl sulfoxide and DMF/*N*-methyl-2-pyrrolidone mixtures, respectively.

1. Introduction

2D perovskites recently attract research interest because of their improved stability and more tunable structural and optoelectronic properties compared to their traditional 3D counterparts.[1–3] While 3D perovskites possess an ABX_3 structure, where the *A* cations fit in the octahedral voids formed by the BX_6 anionic framework, 2D perovskites possess a $R_mA_{n-1}B_nX_{3n+1}$ structure, where *R* is a bulky organic ammonium ion spacer that can be monovalent, forming a Ruddlesden–Popper perovskite (RPP, $m = 2$), or divalent resulting in a Dion–Jacobson perovskite (DJP, $m = 1$).[3] The versatility of 2D perovskites derives from the possibility of changing the organic spacers, which allows us to tune the interlayer interaction in the crystal structure and to change the electronic properties.[4] In addition, another means to tweak the 2D perovskite structure is the variation of *n*, which represents the number of inorganic layers sandwiched between the bulky organic molecules. As widely reported in the literature, tuning *n* leads to a change in the optoelectronic properties of the material, such as bandgap energy and exciton binding energy.[2,3] For solar cell applications, quasi-2D perovskites with *n*-values between 3 and 5 are generally used to achieve a relatively small bandgap, a vertical orientation of the inorganic slabs, which provides a good basis for efficient charge transport, and a smaller exciton binding energy that allows direct generation of free charge carriers instead of excitons, as in the strongly confined (dimensionally and dielectrically) $n = 1$.[5,6] The formation

A. Caiazzo, K. Datta, J. Li, R. Ollearo, M. M. Wienk, R. A. J. Janssen
Molecular Materials and Nanosystems and Institute of Complex Molecular Systems
Eindhoven University of Technology
P.O. Box 513, Eindhoven 5600 MB, The Netherlands
E-mail: r.a.j.janssen@tue.nl

The ORCID identification number(s) for the author(s) of this article can be found under https://doi.org/10.1002/aenm.202102144.

DOI: 10.1002/aenm.202102144

J. Jiang, J. M. Vicent-Luna, S. Tao
Materials Simulation and Modelling
Department of Applied Physics
Eindhoven University of Technology
P.O. Box 513, Eindhoven 5600 MB, The Netherlands

J. Jiang, J. M. Vicent-Luna, S. Tao
Center for Computational Energy Research
P.O. Box 513, Eindhoven 5600 MB, The Netherlands

M. C. Gélvez-Rueda, F. C. Grozema
Department of Chemical Engineering
Faculty of Applied Sciences
Delft University of Technology
Van der Maasweg 9, Delft 2629 HZ, The Netherlands

R. A. J. Janssen
Dutch Institute for Fundamental Energy Research
De Zaale 20, Eindhoven 5612 AJ, The Netherlands

of phase-pure quasi-2D perovskites with a specific *n*-value, however, is an ongoing challenge. Usually, a variety of structural phases with different *n*-values are obtained during film formation, meaning that exploiting the tuneability of quasi-2D perovskite properties (such as bandgap energy tuning) is still not possible.[7] Lately, different processing techniques have been considered to improve the phase purity and solve this issue: among others, solvent engineering has been shown to be a very promising approach.[1,8–10]

Typical solvents for perovskite precursors are *N,N*-dimethylformamide (DMF) and dimethyl sulfoxide (DMSO). The latter is commonly used to improve film morphology via the so-called adduct approach.[11] These polar, aprotic solvents are Lewis bases that form a coordinative bond with Pb^{2+}, which behaves as a Lewis acid.[12] The interactions between solvents and precursors in solution have a strong influence on the crystallization rate and film morphology obtained after spin coating.[13] As a result, the presence of a new organic cation in the perovskite precursor solution, such as provided by the widely used butylammonium iodide (BAI) or phenethylammonium iodide (PEAI) precursors, introduces a new degree of complexity during film formation because the organic spacer ammonium iodides have different interactions with the solvent and PbI_2 than methylammonium iodide (MAI) and thereby influence the crystallization process. This might explain why it is commonly reported in the literature that during the processing of quasi-2D perovskites, many different perovskite structures are formed.[14,15] Even though the stoichiometry of the precursor solution is centered around a specific *n*-value, the resulting perovskite film usually consists of a broad distribution of *n*-values, which may be caused by the different crystallization rates of such perovskite structures.[16] Several studies have investigated the crystallization of quasi-2D perovskites and the current consensus is that nucleation starts at the liquid–air interface.[17–19] Moreover, by using in-situ techniques, it has been recently found that the crystallization is likely to start as a 3D-like perovskite.[18] However, a link between crystallization mechanism and phase distribution in quasi-2D perovskites films has yet to be found.

In 2018, a pioneering study about quantum wells distribution in quasi-2D perovskites highlighted the importance of solvent engineering to tune the phase distribution and crystallinity of such materials.[20] Since then, many reports have studied the effect of solvent mixtures on the composition of quasi-2D perovskites.[19,21–23] In an effort to explain the mechanism behind vertical 2D–3D phase separation in quasi-2D perovskites, Mao et al. studied the effect of DMSO in the precursor solution, finding that a narrower phase distribution with suppression of small-*n* perovskites can be obtained by using 5% DMSO.[24] An intermediate phase derived from the coordination of DMSO with Pb^{2+} was found to be responsible for the suppressed formation of small-*n* phases, as the intermediate was thought to form large-*n* RPPs more easily. On a similar note, Cheng et al. described precursor-solvent interactions as a key factor in determining the phase purity, crystal orientation, and optoelectronic properties, resulting in a power conversion efficiency (PCE) >10% for a propylammonium-based quasi-2D perovskite by tuning the DMF/DMSO ratio in solution.[25] Despite the wide use of DMSO and other co-solvents to enhance the quality of perovskite films, fundamental understanding of how the co-solvents affect the phase distribution is still lacking. Moreover, co-solvents are often assessed by their donor number (D_N) and their coordination ability with Pb^{2+}, without considering their interactions with organic spacers which might be crucially important in explaining phase distribution issues in quasi-2D perovskites. In fact, the aggregation of perovskite precursors, dictated by the formation of an intermediate phase with the co-solvent, might act as a nucleation site and alter the crystallization process drastically.[16] Recently, a large variety of new organic spacers for 2D perovskites are being used to further exploit the potential of this material.[26] Thus, in order to tune phase purity and enhance device efficiency, it is crucial to study the general principles of how these cations interact with solvents in the precursor solution and how such interactions impact the distribution of the *n*-values in resulting films.

In this work, we investigate the crystallization mechanism of quasi-2D perovskite films in the presence of co-solvents and analyze the molecular interactions between different perovskite precursors (MAI, BAI, PbI_2) and solvents (DMF, *N,N*-dimethylacetamide [DMAc], *N*-methyl-2-pyrrolidone [NMP], and DMSO) to correlate such interactions with the resulting phase distribution obtained after film deposition. Additionally, we show that careful tuning of the solvent mixture induces a narrower phase distribution and a less pronounced 2D–3D gradient throughout the thickness of the film, with important implications for the external quantum efficiency (EQE) and performance of solar cells based on quasi-2D perovskites.

2. Results and Discussion

Previous studies in the literature have suggested that crystallization of Ruddlesden–Popper perovskites starts from the liquid–air interface as a 3D-like perovskite.[17,18] Interested in the impact of co-solvents on the crystallization mechanism and phase distribution, we first investigated the kinetics of film formation of quasi-2D perovskite $BA_2MA_3Pb_4I_{13}$ processed from DMF/co-solvent mixtures using in-situ UV–vis–NIR absorption measured in reflection mode conducted during spin coating or thermal annealing (see the Supporting Information for details on the experiment). The perovskite film was processed via room-temperature spin coating, followed by thermal annealing at 100 °C. The $BA_2MA_3Pb_4I_{13}$ composition corresponds to a 2D RPP with an expected *n*-value of $\langle n \rangle = 4$. We selected two high boiling point co-solvents, namely NMP (b.p. 202 °C) and DMSO (b.p. 189 °C), as they effectively slow down the drying rate of the film and allow for a reorganization of the 2D/3D phases in the film. As a comparison, we used DMF (b.p. 153 °C) as pure solvent and a relatively low boiling point co-solvent, such as DMAc (b.p. 165 °C). The perovskite precursors coordinate with these solvents via Lewis acid–base interactions, which, in conjunction with different evaporation rates, impact the crystallization process, as explained later in the text.

The perovskite film turns dark during spin coating only when processed from pure DMF or from a mixture of DMF/DMAc, which have similar boiling points and evaporation rates. **Figure 1**a,d shows that an absorption onset appears after ≈8 s in the 700 nm region when processing the $\langle n \rangle = 4$ perovskite precursor from DMF, indicating formation of a quasi-3D

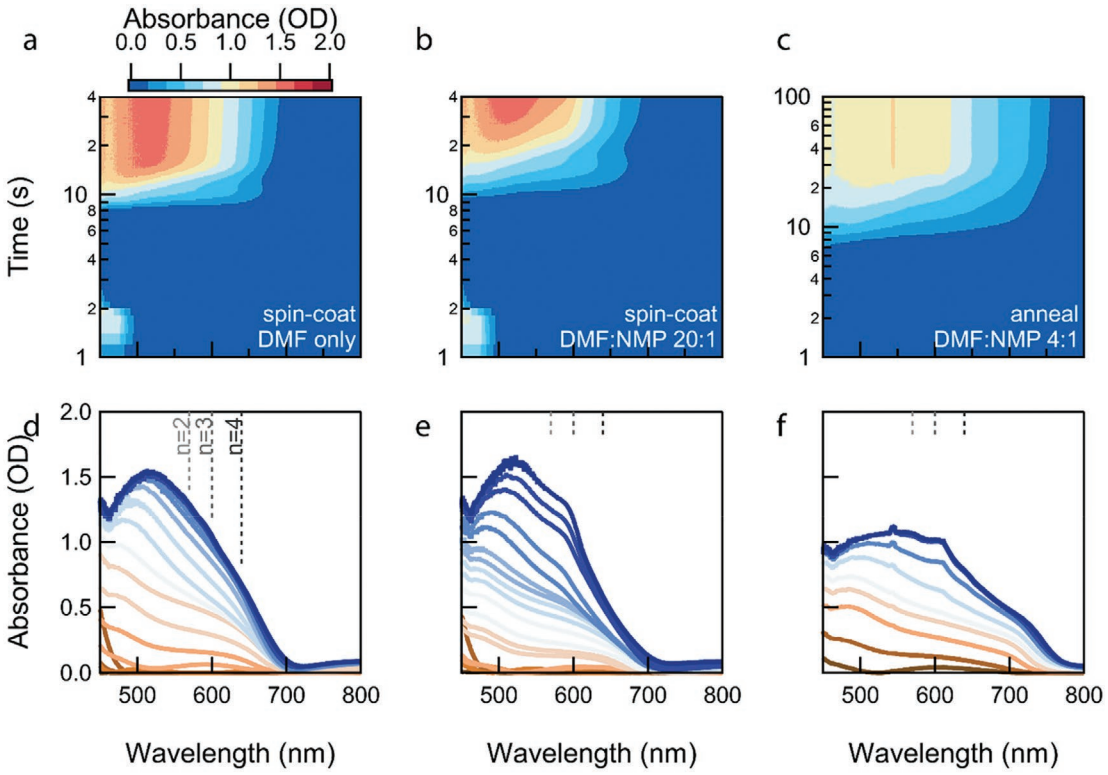

Figure 1. In-situ UV–vis–NIR absorption spectra recorded in reflection mode during spin coating for $BA_2MA_3Pb_4I_{13}$ (<*n*> = 4). a,d) Processed from DMF. b,e) Processed from DMF/NMP (20:1). c,f) In-situ UV–vis–NIR absorption spectra recorded during thermal annealing for $BA_2MA_3Pb_4I_{13}$ (<*n*> = 4) processed from DMF/NMP (4:1). This film did not show any absorption peaks during spin coating, because of the slow crystallization that takes place only during annealing.

perovskite phase soon after spin coating has started. After 35 s, the UV–vis–NIR absorption spectra do not show any additional changes, suggesting completed crystallization during spinning. Interestingly, during spin coating we observe a slight redshift in the absorption onset, which may be representative of perovskite crystal growth to larger *n*-values. Distinct absorption features corresponding to smaller *n*-values are not observed as the film crystallizes. In contrast, when processed from a DMF/NMP 20:1 solvent mixture, the spectrum of a quasi-3D perovskite film develops slightly slower (by ≈2 s) (Figure 1b,e). In this case, after the formation of a quasi-3D perovskite, an excitonic peak at 600 nm, representative of an $n = 3$ phase,[27] begins to appear at 12–13 s. This indicates that the crystallization starts with a quasi-3D phase and is followed by the formation of quasi-2D perovskites, which form slower due to the weak van der Waals interactions between the butyl chains. Similar to the previous case, the absorption onset slightly redshifts with time during spin coating. In an NMP-richer solvent mixture (DMF/NMP 4:1), the film does not turn dark during spin coating, indicating that drying and crystallization of the film is retarded due to the high boiling point of NMP. In this case, a quasi-3D onset at ≈720 nm appears during the first seconds of annealing the film at 100 °C, followed by $n = 2$ (570 nm) and $n = 3$ (600 nm) excitonic peaks[27] (Figure 1c,f). Interestingly, even though the initial quasi-3D onset is observed at 720 nm, the same onset shifts to >750 nm when the quasi-2D perovskite phases are formed. This indicates that the quasi-3D phase at the end of the annealing has become very similar to a $MAPbI_3$ perovskite.[28] Overall, it seems that also under these condition the crystallization of a 3D perovskite is kinetically more favorable and implies that the formation of a phase-pure quasi-2D perovskite is challenging because the presence of MA inevitably leads to a fast crystallization of quasi-3D perovskites. Similar behavior is observed when using DMSO as a co-solvent (Figure S1, Supporting Information). The addition of high boiling point co-solvents therefore effectively slows down the crystallization of the perovskite film. Moreover, slow crystallization influences the phase distribution of the resulting film: when pure DMF is used, mostly a quasi-3D perovskite with undefined *n*-value is formed because the 2D perovskite phase crystallizes too slow to form a distinct 2D–3D gradient. When using high boiling point co-solvents, instead, distinct 2D and 3D phases are formed. Notably, we also find that such a 3D-like perovskite seems to form larger *n*-values over time, indicating that the top part of the film might still be influenced by the ongoing crystallization of the small-*n* phases at the bottom.

To investigate changes in the formation of different structural phases and their distribution across the thickness of the film, the perovskite films processed from DMF/co-solvent mixtures were characterized by optical spectroscopy. **Figure 2**a shows the UV–vis–NIR absorption spectra of quasi-2D $BA_2MA_3Pb_4I_{14}$ (<*n*> = 4) perovskite films processed from precursor solutions containing pure DMF or DMF/co-solvent mixtures. The films processed from DMF/NMP and DMF/DMSO display more

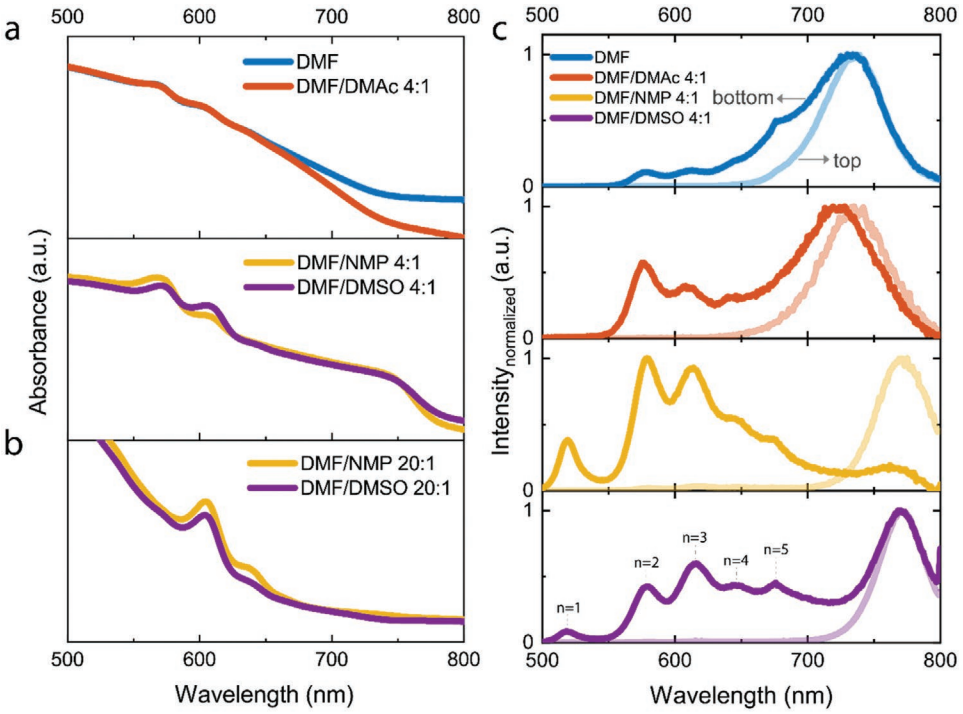

Figure 2. Optical characterization of $BA_2MA_3Pb_4I_{13}$ ($<n> = 4$) quasi 2D-perovskite layers on glass substrates. a) UV–vis–NIR spectra of films processed from DMF/co-solvent 4:1 (v/v). b) Same as panel (a), but for films processed from DMF/co-solvent 20:1 (v/v). c) Normalized steady-state PL spectra of films processed from DMF/co-solvent 4:1 (v/v) with excitation at 405 nm from the air/perovskite (top) and substrate/perovskite (bottom) interface side.

clear signals of 2D phases and distinct, redshifted absorption onsets for the 3D perovskite compared to the spectra of layers processed from DMF/DMAc or pure DMF. With a bandgap of ≈1.63 eV, the quasi-2D perovskites processed from DMF/NMP and DMF/DMSO seem to induce the formation of an almost pure 3D perovskite phase in parts of the film, compared to the formation of quasi-3D perovskite phases with higher bandgap in the films processed from DMF and DMF/DMAc (1.72 and 1.77 eV, respectively).

The formation of a 3D perovskite phase is also evident from steady-state photoluminescence (PL) spectra (Figure 2c), which show one main 3D emission peak when films are excited at 405 nm from the perovskite (top) side. The PL maximum is shifted to longer wavelengths in case of DMF/NMP and DMF/DMSO. The difference in the bandgaps can also be determined from the PL maxima, which are found at ≈1.68 eV for DMF and DMF/DMAc compared to 1.61 eV for DMF/NMP and DMF/DMSO. As mentioned before, the latter values are similar to the emission of $MAPbI_3$.[28] In the 500–650 nm region of the UV–vis–NIR spectra, the films processed with all solvent mixtures display excitonic absorption peaks associated with (quasi-) 2D perovskite structures with different *n*-values.[27] The absorption spectra indicate that the co-solvent has an impact on the phase distribution of the small-*n* phases because the quasi-2D perovskite film processed from DMF/NMP shows a strong excitonic peak for the $n = 2$ phase at 570 nm, with relatively smaller peaks for $n = 1$ at 515 nm and $n = 3$ at 610 nm,[27] whereas the perovskite processed from DMF/DMSO display a strong excitonic peak for $n = 3$ and low intensity for $n = 2$ and $n = 4$ (640 nm). UV–vis–NIR spectra of films processed with DMF only and DMF/DMAc are relatively similar with a shallow absorption onset for the 3D perovskite phase and weak excitonic peaks. A sharper 3D perovskite absorption onset, as seen with NMP and DMSO as co-solvents, is therefore associated with higher intensities for the excitonic peaks of the small-*n* perovskites. Once a 3D perovskite is formed, the excess BA^+ cations will lead to the formation of quasi-2D perovskites with smaller *n*-values.

As is commonly reported in the literature, quasi-2D perovskite films show different PL spectra when excited from the air/perovskite (top) or substate/perovskite (bottom) interfaces, as a result of a vertical 2D–3D phase distribution in the film. The normalized PL spectra of the quasi-2D perovskite films confirm this vertical phase separation (Figure 2c). The film processed from DMF exhibits weak PL peaks at 560, 605, 640, and 680 nm, corresponding to 2D phases with $n = 2$, 3, 4, and 5[29] when excited from substrate (bottom) side but no sign of 2D phase emission when excited from the air (top) side. This indicates that the 3D phase is confined at the top of the film and the 2D phases at the bottom. The co-solvents strongly influence the phase distribution of 2D phases at the substrate side. Compared to pure DMF, films processed from DMF/DMAc result in an enhanced emission for the 2D phases with $n = 2$ to 4 with bottom excitation. The film processed from DMF/NMP shows peaks at 520, 580, 615, 645, and 675 nm, corresponding to quasi-2D phases with $n = 1$ to 5.[29] The most intense PL peak is found for the 2D phase with $n = 2$ and there is only a small peak for the 3D phase. Finally, the film processed from DMF/DMSO also displays the PL emissions for $n = 1$ to 5, but the phase distribution is shifted towards larger *n*-values compared

to NMP, and the 3D phase PL peak has the highest intensity. While these largely different PL spectra certainly point towards different phase distributions for different co-solvents, a quantitative analysis of the phase distribution is hampered by the several unknown factors, such as the absorption coefficient and PL quantum yields of different phases and the extent to which emission occurs after migration of charge carriers to low-bandgap regions.

The presence of a vertical 2D–3D phase separation is confirmed by angle-dependent grazing-incidence wide-angle X-ray scattering (GIWAXS) measurements. The angle of incidence α was varied from 0.1° to 0.5° to gain depth sensitive information about the film. At angles below 0.2°, only the top 10–20 nm of the film are analyzed, while the X-rays penetrate the full thickness of the film at higher angles.[30] Because the PL spectra indicate that the 2D phases are most prominent in films processed from DMF/NMP we investigated the vertical phase distribution of these films (Figure S2, Supporting Information). With $\alpha = 0.1°$ and 0.2°, the quasi-2D perovskite film processed from DMF/NMP 4:1 resembles a well-oriented 3D perovskite, while with $\alpha > 0.2°$ new Bragg spots appear in the out-of-plane direction at 0.2 and 0.3 $Å^{-1}$, which are associated with the $n = 3$ and $n = 2$ (020) planes.[31] To have a better picture at small q values, we also measured grazing-incidence medium-angle X-ray scattering (GIMAXS) on the same film (Figure S3, Supporting Information), which shows a clear Bragg spot at $q = 0.32$ $Å^{-1}$, associated to the (020) plane of an $n = 2$ quasi-2D perovskite, appearing when probing with $\alpha = 0.3°$ or higher. These results confirm that small-n phases are formed mainly at the bottom of the film, as also observed via PL spectroscopy, when processed with relatively high amount of NMP in the precursor solution.

Based on the optical characterization and GIWAXS, we can conclude that our in-situ UV–vis–NIR absorption measurements are in good agreement with previous reports in suggesting that the crystallization starts from the liquid/air interface as a 3D-like perovskite, even with the presence of a high boiling point co-solvent. In fact, in-situ UV–vis–NIR absorption measurements during spin coating or thermal annealing indicated that the perovskite crystallization starts as a quasi-3D perovskite, while PL and angle-dependent GIWAXS located such phases at the top of the film, implying that the crystallization starts from the top.

To investigate if the optical quality of the films can be improved and scattering of light can be reduced, lower amounts of NMP and DMSO in DMF were used, which enhanced the drying rate. The UV–vis–NIR spectrum of $BA_2MA_3Pb_4I_{13}$ ($<n> = 4$) films processed from DMF/NMP 20:1 and DMF/DMSO 20:1 reveal that the use of NMP and DMSO in smaller amounts with DMF is efficient in producing a more phase-pure film that shows only excitonic peaks for $n = 3$ and 4, no pronounced 3D onset, and much less scattering (Figure 2b). This 20:1 solvent/co-solvent ratio provides an optimal crystallization rate where the arrangement of rather pure 2D and 3D phases is neither absent, as in the case of the 1:0 ratio, nor as distinct as observed when using the 4:1 ratio. As a result, the crystallization kinetics is driven to the formation of a relatively phase-pure quasi-2D perovskite. However, while the stoichiometry of the precursor solution was selected to make an $n = 4$ quasi-2D perovskite, the phase distribution for these films seem to be centered around $n = 3$ with a prominent peak at 605 nm. The PL spectra of these films still show emission peaks corresponding to 2D phases with $n = 3$ and 4, but are dominated by the 730 nm peak related to a quasi-3D perovskite phase (Figure S4, Supporting Information). Peaks that are due to $n = 1$ and 2 are largely absent. This result suggests that a more phase-pure 2D might have been formed but that a certain amount of quasi-3D perovskites is still present. The strong PL emission in the 700–800 nm region might originate from efficient charge transport from small-n phases to the quasi-3D phase, which might lead to a dominant PL emission arising from a quasi-3D phase with lower bandgap energy, even if the latter is present only in small amounts in the film. Because of this, it is not possible to use the PL spectra to quantitatively determine the amounts of different phases in the film. Instead, we rely on UV–vis–NIR spectra and determine that the quasi-3D perovskite phase must be present in small concentrations as indicated by the very shallow onset in the 700 nm region and that we are able to fabricate a reasonably phase-pure quasi-2D perovskite by carefully tuning the DMF/co-solvent ratio.

To gain more understanding of the dynamics of charge carriers and to quantitatively investigate the phase distribution in the films with optimized n-value distribution, we measured ultrafast transient absorption (TA) for $BA_2MA_3Pb_4I_{13}$ ($<n> = 4$) perovskite films processed from DMF and DMF/NMP 20:1. **Figure 3**a,b displays the TA spectra at different decay times after top and bottom excitation, respectively, for the reference film processed from pure DMF. After excitation from the perovskite (top) side, the TA spectrum displays ground state bleaching (GSB) of $n = 2$ to 4 and quasi-3D perovskites, followed by an ultrafast bleach recovery for the small-n phases and a concomitant rise of the GSB peak for quasi-3D perovskite at 720 nm. This indicates fast (<1 ps timescale) and efficient carrier migration from the quasi-2D perovskites phases to the quasi-3D phase. As also suggested by the PL spectra, a 2D–3D vertical phase separation is observed in the TA spectra, where excitation from the substrate (bottom) side leads to much more intense GSB peaks for $n = 2$ (570 nm), $n = 3$ (605 nm), $n = 4$ (640 nm), and $n = 5$ (665 nm), with no bleaching in the 700 nm region. In a timescale of less than 1 ps, we observe a sequential bleaching and recovery for $n > 2$ perovskites, suggesting carrier migration from small-n to large-n perovskites,[32] as indicated by a GSB peak at 700 nm, which reaches its maximum at ≈50 ps. This peak is found at shorter wavelength compared to the quasi-3D GSB peak observed after top illumination, thus it is related to a perovskite phase with a lower, unidentified large n-value. After 50 ps, decay from all perovskite phases is observed, although it is worth noting that the charge carrier transfer does not seem complete, as GSB peaks are still observed for $n = 2$ to 4 at 50 ps and they simply decay together with the larger-n peak. The TA spectra of the $BA_2MA_3Pb_4I_{13}$ film processed from DMF/NMP (20:1) display $n = 3$ to 6 and quasi-3D GSB peaks (Figure 3c,d), confirming that $n = 1$ and 2 phases are not formed, in agreement with the UV–vis and PL spectra. Moreover, top- and bottom-excitation TA spectra (Figure 3c,d) seem to indicate a more homogeneous phase distribution where $n = 3$ to 6 quasi-2D perovskites are located throughout the whole thickness of the film. This suggests that by optimizing the DMF/co-solvent ratio it is possible to avoid a strong 2D–3D vertical

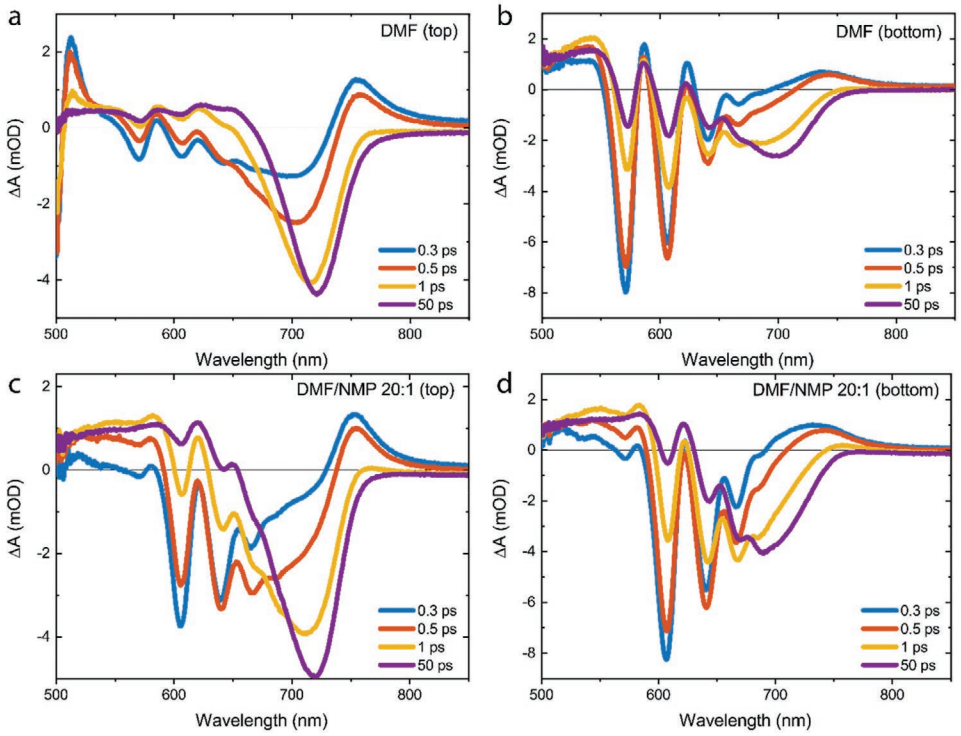

Figure 3. Ultrafast transient absorption (TA) spectra of $BA_2MA_3Pb_4I_{13}$ (<*n*> = 4). a,b) Films processed from DMF and excited from air/perovskite (top) and substrate/perovskite (bottom) side, respectively. c,d) Films processed from DMF/NMP 20:1 and excited from top and bottom side, respectively.

phase separation, even though it seems that a certain degree of such separation is inevitable. The TA spectrum from bottom excitation, in fact, displays only n = 3 to 6 GSB peaks, located at 605, 640, 665, and 690 nm, and no clear quasi-3D perovskite absorption at 0.3 ps delay time. In contrast, top excitation shows slightly higher absorption in the quasi-3D region at 720 nm, which suggests formation of quasi-3D phases preferentially at the top of the film and a narrower phase distribution at the bottom. This might explain the ultrafast charge carrier migration from quasi-2D to quasi-3D in the top excitation TA spectrum, which shows an ultrafast rise of the quasi-3D bleach peak that dominates the spectrum after just 1 ps. From bottom excitation, we again observe a sequential bleach and recovery for the quasi-2D phases, although on a longer timescale, as can be seen from the n = 3 to 6 peaks still present at 50 ps. We speculate that the slower carrier transfer after bottom excitation might be related to the fact that less or no quasi-3D phases are present at the bottom of the perovskite film, thus leaving no space for an ultrafast carrier transfer that is instead observed after top excitation.

We further investigated the crystal structure and orientation of the quasi-2D perovskite films with X-ray diffraction (XRD) and GIWAXS. **Figure 4**a shows the XRD diffraction patterns of $BA_2MA_3Pb_4I_{13}$ (<*n*> = 4) films processed from DMF/co-solvent 4:1. DMSO and NMP are effective in improving the orientation and crystallinity of the film in the out-of-plane direction, as indicated by the drastic enhancement in intensity of the peaks at 14° and 28°, assigned to (111) and (202) planes of RPP or (quasi-)3D perovskites,[33] and by the full width at half maximum (FWHM) of the (111) peak decreasing from 0.56° and 0.26° for DMF and DMF/DMAc, respectively, to 0.12° and 0.16° for DMF/NMP and DMF/DMSO. In addition, a set of (0*k*0) peaks in the 3–10° region is observed in the diffraction patterns of the films processed with NMP and DMSO, which indicates the formation of parallel-oriented small-*n* quasi-2D phases. For instance, the peaks at 3.4° and 4.4° are assigned to n = 3 and n = 2 quasi-2D perovskite (020) planes, respectively. The XRD diffraction patterns confirm the prevalence of n = 3 phases in the DMF/DMSO-processed films and of n = 2 phases in the DMF/NMP-processed samples, in agreement with the optical characterization. Some (0*k*0) peaks are also found in the DMF and DMF/DMAc films, although the peaks are not sharp and of low intensity. Interestingly, while the perovskite processed with DMF and DMF/DMAc retain such parallel-oriented RPPs even when using the optimized 20:1 ratio (Figure 4b-inset), films processed with DMF/NMP (20:1) and DMF/DMSO (20:1) do not show any (0*k*0) peaks if the co-solvent is present in small amounts in the precursor mixture. Remarkably, the addition of NMP is found to drastically increase (≈30×) the intensity of the (202) peak, compared to the diffraction pattern of the film processed in DMF only. In addition, the ratio $I_{(202)}/I_{(111)}$ increases from 0.61 and 0.81 for DMF and DMF/DMAc to 2.36 and 1.39 for DMF/NMP and DMF/DMSO, thus indicating a preferential out-of-plane crystal growth with the use of the latter co-solvents.[34] Figure 4c–h displays the GIWAXS measurements for the quasi-2D perovskite films processed from DMF and DMF/co-solvent combinations with 4:1 and 20:1 volume ratios. The film processed from pure DMF exhibits scattered rings (Figure 4c), which suggests a random orientation of the crystals. Moreover, a weak Bragg spot at q_z = 0.3 Å^{-1} (020) indicates the presence of an n = 2 phase oriented parallel with

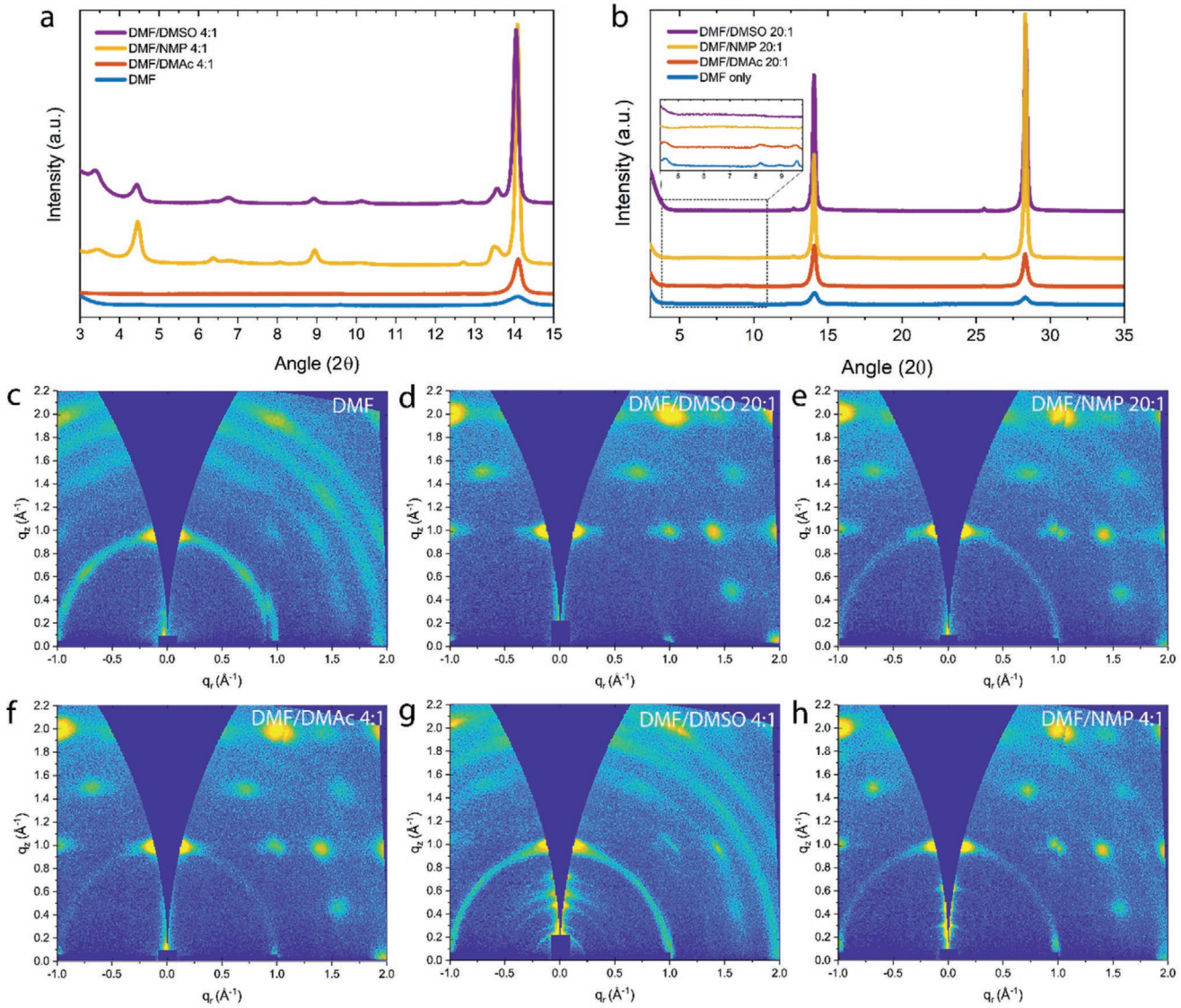

Figure 4. a,b) XRD diffraction patterns for $BA_2MA_3Pb_4I_{13}$ ($<n> = 4$) films processed in DMF/co-solvent 4:1 and DMF/co-solvent 20:1 mixture, respectively. c–h) GIWAXS patterns for $BA_2MA_3Pb_4I_{13}$ ($<n> = 4$) films processed in a variety of solvent mixtures, as indicated on top of each plot.

respect to the substrate. In contrast, films processed with small amounts (20:1 ratio) of NMP and DMSO display discrete Bragg spots (Figure 4d,e), indicating an enhanced crystal orientation in the out-of-plane direction, as also inferred from XRD, that might be beneficial for charge transport, and no spots associated to parallel-oriented small-n quasi-2D phases.[35,36] As the insulating large organic spacers do not allow for charge carriers to be transported, a favorable orientation of the crystals in quasi-2D perovskites is thought to be beneficial for charge collection and device efficiency. As mentioned above, addition of co-solvents in larger amounts (DMF/co-solvent ratio 4:1) induces a strong 2D–3D phase separation. The film processed in DMF/DMSO 4:1 shows again azimuthal spreading of the diffracted intensity at $q = 1$ Å^{-1} (Figure 4g), thus indicating that a larger amount of DMSO, compared to the ratio DMF/DMSO 20:1, is not beneficial anymore in enhancing the crystal orientation. In addition, the small-angle region exhibits many Bragg spots related to small n-values quasi-2D perovskites. Such small-n phases are oriented parallel to substrate and inhibit charge transport. Interestingly, the $n = 3$ phase ($q = 0.2$ Å^{-1}) shows a noticeable ring apart from an intense Bragg spot along the out-of-plane direction, which denotes the tendency of phases with $n > 2$ to orient also in non-parallel directions with respect to the substrate. Moreover, in agreement with XRD, the out-of-plane cut (Figure S5, Supporting Information) shows a peak at $q_z = 0.24$ Å^{-1}, which is—as mentioned above—indicative of an $n = 3$ quasi-2D perovskite phase, that is drastically more intense than the $n = 2$ phase, indicating prevalence of perovskites with such n-value. On the contrary, perovskite films processed from DMF/NMP 4:1 (Figure 4h) and DMF/DMAc 4:1 (Figure 4f) retain enhanced crystal orientation, even though small-n peaks are clearly visible for films processed with NMP, in agreement with optical characterization. In the latter case, the out-of-plane cut displays both peaks related to $n = 2$ and $n = 3$, with the former being more intense. Overall, the use of these

co-solvents seems to induce vertical orientation in the films, possibly because the interaction of the co-solvents with the perovskite precursors does not allow the formation of a monolayer of butylammonium molecules at the liquid–air interface, which would lead to a parallel orientation.[17]

The analysis of the phase distribution obtained via optical and X-ray characterization reveals that by using different high boiling point co-solvents, the distribution of *n*-values is shifted. More specifically, we have observed that by using NMP or DMSO as a co-solvent with DMF in a 1:20 ratio, a more phase-pure quasi-2D perovskite film can be fabricated, whereas by using a 1:4 ratio, the phase distribution is centered around $n = 2$ and $n = 3$, respectively. Understanding why some co-solvents lead to different phase distributions is important to make new design rules for the choice of solvent mixtures in quasi-2D perovskites processing. A recent study has identified the perovskite precursor phases that are present in the sol-gel state before crystallization and by mapping the possible reaction pathways, the authors proposed a mechanism where the precursor phases likely react with free BAI or MAI molecules to form the perovskite.[18] When a co-solvent is present in the solvent mixture, however, the availability of MAI and BAI in solution might be different. In fact, MAI or BAI might interact differently in the solvent-PbI_2-MAI(BAI) complexes that are likely present in solution and be more or less bound to them. The different interactions of BAI and MAI with PbI_2 and solvents in solution might explain the change in phase distribution, as this would influence how easy it is for a BAI or MAI molecule to react with the precursor phase to form a perovskite.

To verify whether this hypothesis is valid, we analyzed the interaction of ternary complexes MAI(BAI)–PbI_2–solvent (DMF, NMP, DMSO) by measuring the Fourier transform infrared (FTIR) spectra (**Figure 5**a–c). In the case of DMF, the C=O stretching peak broadens and its maximum shifts from 1659 cm^{-1}

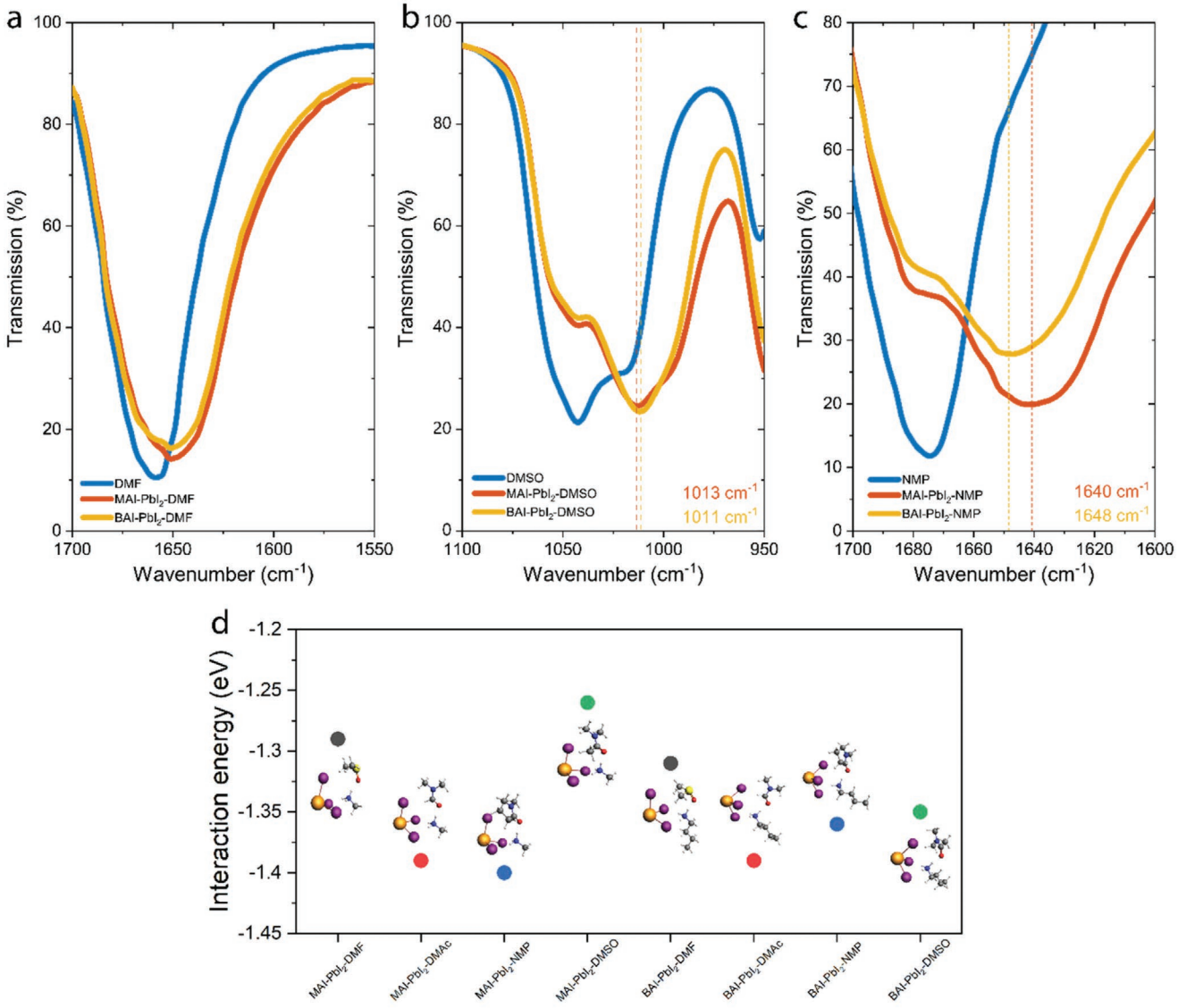

Figure 5. a–c) FTIR spectra of perovskite precursor solutions composed of BAI (MAI), PbI_2, and solvent. The reference spectrum for the pure solvent is displayed in each plot, respectively. d) Molecular interaction of MAI or BAI ternary complexes formed with PbI_2 and solvents.

for pure DMF to 1651 cm^{-1} after addition of PbI_2 and MAI or PbI_2 and BAI. The shift indicates that the C=O bond weakens by the interaction with the perovskite precursors.[37,38] The broadening can be due to the coalescence of the peaks of pure DMF at 1659 cm^{-1} and one at lower wavenumbers for the DMF-PbI_2-MAI and DMF-PbI_2-BAI complexes. The C=O peak shifts by the same amount (8 cm^{-1}) when using MAI and BAI, indicating that there is no significant difference for these organic ions. The C=O stretch vibration of NMP undergoes a similar change, but in this case two separate signals are observed in the mixtures, one for pure NMP at 1679 cm^{-1} and one at lower wavenumbers for the NMP-PbI_2-MAI and NMP-PbI_2-BAI complexes. Interestingly, the MAI complex shifts the C=O peak to 1640 cm^{-1}, whereas the BAI complex to 1648 cm^{-1}. This suggests that the C=O bond from NMP is more weakened when it interacts with MAI-PbI_2 compared to BAI-PbI_2, indicating that NMP interacts more strongly with MAI-PbI_2. Finally, in the case of DMSO, the S=O stretching peak shifts from 1043 cm^{-1} for bare DMSO to 1013 and 1011 cm^{-1} after addition of MAI-PbI_2 and BAI-PbI_2, indicating that a slightly stronger interaction might be found with the BAI complex, contrarily to what is observed with NMP. As a result, when using NMP as a co-solvent it seems that MAI is strongly bound in the MAI-PbI_2-NMP complex, thus making it easier for the precursors in the sol-gel state to react with BAI and to shift the phase distribution towards small-*n* phases. On the other hand, when using DMSO the picture tends to a certain extent to be reversed, and a broader phase distribution might be facilitated.

Furthermore, we calculated the interaction energies of PbI_2, MAI, and BAI with the three solvents (DMF, NMP, and DMSO) (Figure 5d) via DFT calculations. We adopted the molecular structure of [MA^+(BA^+)–PbI_3^-–solvent]. The configuration is one of the most favorable out of thousands tested by using the combination of Monte Carlo and density functional theory (MC–DFT) scheme (Figure S6, Supporting Information). This structure has been successfully applied in a previous study to evaluate the interaction strength of FA^+–PbI_3^-–solvent.[13] The interaction energies of MAI (BAI)–PbI_2–DMSO are E_{inter} = −1.26 and −1.35 eV, respectively, indicating that MAI interacts more weakly in a complex with DMSO and PbI_2 compared to BAI. On the contrary, the complex formed by MAI, PbI_2, and NMP has a slightly stronger interaction energy compared to the BAI complex (−1.40 versus −1.36 eV). More details about these calculations can be found in Table S1, Supporting Information. We also performed a vibration frequency analysis of the ternary complexes and found the same trend as we observed from the FTIR experiments (Figure S7, Supporting Information), namely a shift to lower wavenumbers for the BAI-PbI_2-NMP complex compared to MAI and vice versa for DMSO. We additionally performed FTIR experiments and DFT calculations also for the binary complexes (MAI or BAI with solvents, or PbI_2 with solvents), which are displayed in Figures S8 and S9, Supporting Information. The interaction of the solvents with PbI_2 is confirmed by the shift of the C=O or S=O peak to lower wavenumbers; in the case of NMP, a larger shift is found compared to DMF, which is in agreement with the higher donor number of NMP. The same peaks shift when adding only the organic salts (i.e., BA or MA) to the solvents, although in this case the shifts are equal for both spacers.

Overall, to explain all the results described above, we propose a mechanism where the crystallization of the quasi-2D perovskite film starts at the liquid/air interface as a quasi-3D perovskite. Depending on the content of DMSO or NMP, such crystallization starts during spin coating or during annealing. While the crystallization proceeds, BAI and MAI molecules react to keep forming a perovskite layer. However, the availability of BAI and MAI molecules in the wet film is not the same, as they might interact differently with the co-solvent that has yet to evaporate. This affects the *n*-values distribution that is found at the bottom of the film, in the way described via optical and X-ray characterization. The use of NMP allows a phase distribution more shifted to small *n*-values, such as n = 2, because BAI interacts less in solution and is more available to react, whereas the use of DMSO shifts the distribution to slightly larger *n*-values.

Finally, using the new insights obtained by tuning the DMF/DMSO and DMF/NMP ratios to achieve relatively phase-pure quasi-2D perovskites, we fabricated planar *p–i–n* solar cell devices. The quasi-2D $BA_2MA_3Pb_4I_{13}$ (<*n*> = 4) perovskite was processed on a glass substrate covered with a patterned transparent indium tin oxide (ITO) electrode and a poly[bis(4-phenyl)(2,4,6-trimethylphenyl)amine] (PTAA) hole-transport layer, and then sandwiched by thermally-evaporated C_{60} and bathocuproine (BCP) electron-transport layers and an Al back electrode (glass/ITO/PTAA/quasi-2D $BA_2MA_3Pb_4I_{13}$ (<*n*> = 4)/C_{60}/BCP/Al) (**Figure 6**b). Figure 6c,d displays the current density–voltage (*J–V*) characteristics recorded with AM1.5G (100 mW cm^{-2}) illumination and the EQE spectra of the $BA_2MA_3Pb_4I_{13}$ (<*n*> = 4) based devices, while **Table 1** summarizes the relevant solar cell parameters. The quasi-2D perovskites processed only in DMF and in DMF/DMAc 20:1 lead to poor photovoltaic devices with PCEs of 3.5% and 5.2%, respectively. Optimized devices processed from DMF/NMP and DMF/DMSO with ratio 20:1 display dramatically enhanced solar cell parameters, reaching efficiencies of 10.2% and 11.1%, respectively, which are reproducible over many devices (Figure S10, Supporting Information). Moreover, the hysteresis index (HI) of the solar cells fabricated with optimized quasi-2D films is calculated as 0.07, much lower than the HI of the cells with active layer processed from DMF and DMF/DMAc solvent mix (0.19 and 0.15, respectively). The most prominent increase in the solar cells is reported for the short-circuit current density, which is more than doubled after addition of NMP and DMSO in the solvent mixture, even though this is also accompanied by an increase in both open-circuit voltage (V_{OC}) and fill factor (FF). We attribute the increase in solar cell performances to the absence of n = 1 and 2 phases in the optimized films, which are usually oriented parallel to the substrate and inhibit charge transport, and by the enhanced crystallinity and more favorable crystal orientation. Via solvent engineering, we show that it is possible to have a certain degree of control over these important parameters in quasi-2D perovskites, as schematically represented in Figure 6a. To support this, we measured transient photocurrent (TPC) on devices with active layers processed from all solvent mixtures, as shown in Figure 6e. As expected, devices processed with DMF or DMF/DMAc, which display a less homogeneous phase distribution, show a longer decay time (τ) of the photocurrent equal to 7 and 14 µs, respectively,

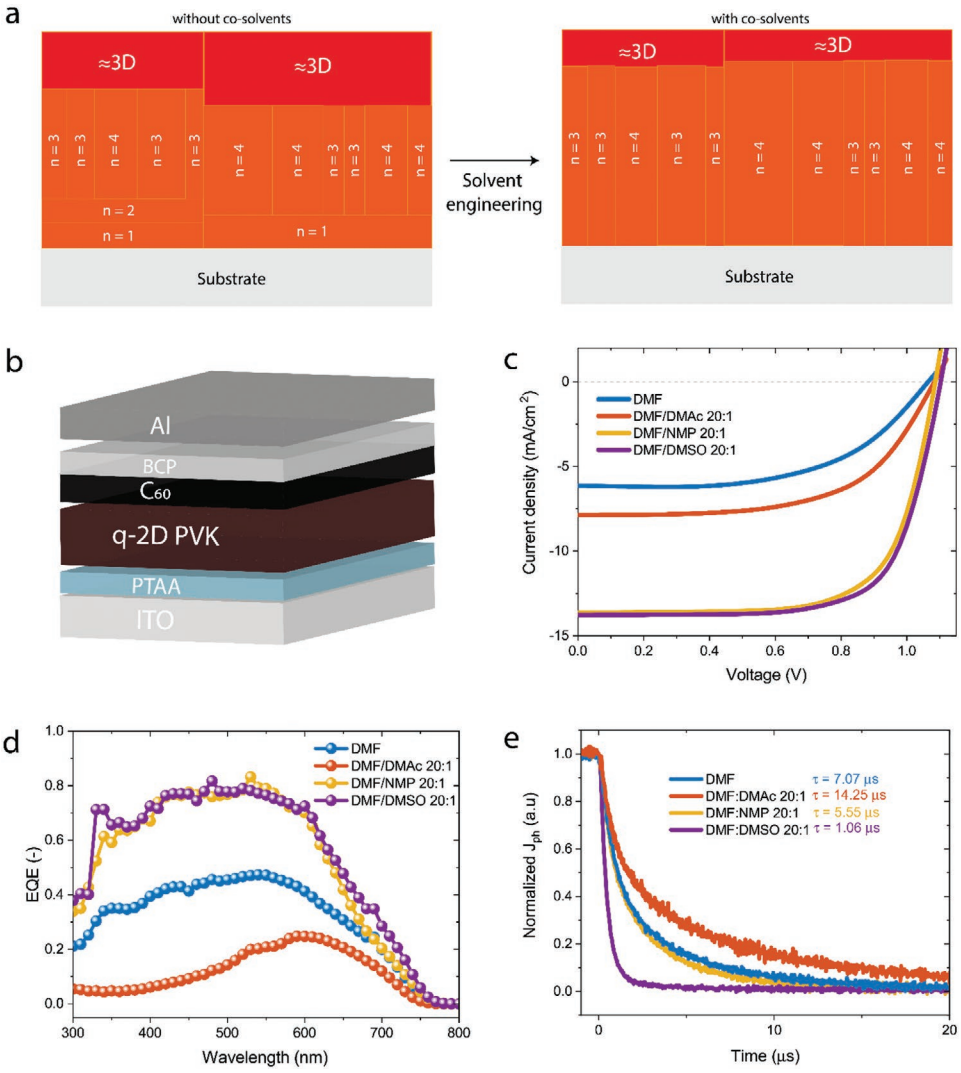

Figure 6. a) Schematic illustration quasi-2D perovskite film composition before and after tuning of the DMF/co-solvent ratio. b) Schematics of the solar cell configuration used for devices. c) *J–V* characteristics for solar cells based on $BA_2MA_3Pb_4I_{13}$ ($\langle n \rangle = 4$) active layer and processed from DMF/co-solvent mix 20:1, recorded with simulated AM1.5G (100 mW cm^{-2}) light. d,e) EQE spectra and TPC measurements for the abovementioned solar cell devices.

possibly because 2D crystallites are orientated parallel to the surface and because phase impurity leads to difficulties in extracting charge carriers. On the other hand, the optimized devices processed with DMF/NMP or DMF/DMSO display a shorter decay time, with τ reaching 5 and 1 µs, respectively. This is in line with the better crystal orientation and more homogeneous phase distribution, which makes charge carriers extraction easier. A more pronounced vertical orientation in the films processed with DMF/DMSO, as indicated by the less noticeable ring at $q = 1$ $Å^{-1}$ in Figure 4d, is consistent with the shorter decay time for such devices, compared to the ones processed in DMF/NMP. The EQE spectra, displayed in Figure 6d, show a drastic enhancement in quantum efficiency for devices processed with DMF/NMP and DMF/DMSO, reaching 80% in

Table 1. Solar cell parameters for $BA_2MA_3Pb_4I_{13}$ ($\langle n \rangle = 4$) active layers processed from DMF/co-solvent (20:1) mixtures. The thickness of the active layers is comparable (±15 nm).

	$J_{SC,EQE}$ [mA cm^{-2}]	V_{OC} [V]	FF [–]	PCE [%]	Hysteresis index
DMF	6.0	1.06	0.56	3.5	0.19
DMF/DMAc 20:1	8.1	1.08	0.60	5.2	0.15
DMF/NMP 20:1	13.5	1.09	0.70	10.2	0.07
DMF/DMSO 20:1	14.2	1.10	0.71	11.1	0.07

the 400–600 nm range, while much poorer performances are observed for other devices. In addition, we observe an onset at 750 nm for all devices, which is an indication of the formation of a quasi-3D perovskite phase. This onset clearly shows that even though phase purity is better for optimized films, in terms of vertical phase separation and absence of small-*n* structures, there is always the formation of a certain amount of 3D-like perovskite. Very commonly in the literature, such onset in the EQE spectra is not considered as evidence of impurity in what are often wrongly considered phase-pure quasi-2D perovskite devices. Finally, in agreement with the analysis of the interaction energies of the precursor intermediates, we observe that perovskites processed from DMF/DMSO 20:1 display a slightly broader shoulder in the 700 nm region, which seems to confirm the assumption that DMSO leads more easily to the formation of quasi-3D perovskites compared to NMP. The PCEs for the $BA_2MA_3Pb_4I_{13}$ ($<n> = 4$) perovskite solar cells of 10.2% (from DMF/NMP 20:1) and 11.1% (from DMF/DMSO 20:1) are somewhat less than the PCE of 13.3% recently reported by Zhang et al. for the same perovskite processed from DMF/DMSO (97:3).[39] While the solar cells presented here have higher FF and similar V_{OC}, their current density is lower, because of a slightly lower and blue-shifted onset of the EQE. The latter indicates better phase purity but is not yet accompanied by the higher V_{OC} that would be expected for a phase-pure wide bandgap 2D perovskite.

3. Conclusions

In summary, we have demonstrated that the perovskite precursor solution plays an important role in determining the phase distribution in quasi-2D perovskite films and that consequently, solvent engineering is a viable strategy to improve phase purity and device efficiency. Carefully tuning the solvent mixture led to an improvement in the efficiency of solar cells using a BA $<n = 4>$ perovskite active layer from 3.5% when using no co-solvent to 11.1% and 10.2% when processed from DMF/DMSO and DMF/NMP mixtures, respectively. We noticed an enhancement in crystallinity and crystal orientation, together with a narrower 2D–3D phase distribution, which is beneficial for charge carrier extraction. Moreover, we confirmed that the crystallization of quasi-2D perovskite films starts from the liquid/air interface as a quasi-3D perovskite, even in the presence of high boiling point co-solvents, and proceeds to form quasi-2D perovskite phases on the bottom of the film. Each co-solvent, however, influences the distribution of *n*-values differently. By investigating the solvent-precursors interaction energies via FTIR and DFT, we confirmed that the phase distribution is indeed influenced by the co-solvents due to a difference between the interaction of MA (or BA) and PbI_2 with the co-solvents. As the perovskite crystallization proceeds, the availability of MA and BA to react is different because the organic ions interact more or less strongly with the co-solvents, which leads to a shift of the phase distribution towards small *n*-values in the case of NMP and to a broader distribution of structural phases when using DMSO. Our results indicate that a careful analysis of the precursor solution is a good starting point to tune the phase distribution of quasi-2D perovskites. In particular, new organic spacers might interact in a different manner with PbI_2 and the solvents, compared to MAI; thus, the use of new solvent mixtures or additives might be crucial to develop an efficient and phase-pure quasi-2D perovskite with unconventional spacers.

Supporting Information

Supporting Information is available from the Wiley Online Library or from the author.

Acknowledgements

The research has received funding from the Ministry of Education, Culture and Science (Gravity program 024.001.035) and the Netherlands Organization for Scientific Research via a Spinoza grant. The authors acknowledge the Netherlands Organization for Scientific Research (NWO) for funding through the Joint Solar Programme III (project 680.91.011). The research leading to these results in the Delft University of Technology has received funding from the European Research Council Horizon 2020 ERC Grant Agreement no. 648433. S.T. and J.J. acknowledge funding by the Computational Sciences for Energy Research (CSER) tenure track program of Shell/NWO (Project number 15CST04-2); S.T. and J.M.V.-L. acknowledge funding from NWO START-UP program, The Netherlands.

Conflict of Interest

The authors declare no conflict of interest.

Data Availability Statement

The data that support the findings of this study are available from the corresponding author upon reasonable request.

Keywords

crystallization, film formation, Ruddlesden-Popper perovskites, solvent engineering, solar cells

Received: July 14, 2021
Revised: August 15, 2021
Published online: October 5, 2021

[1] A. Z. Chen, J. J. Choi, *J. Vac. Sci. Technol., A* **2020**, *38*, 010801.
[2] G. Grancini, M. K. Nazeeruddin, *Nat. Rev. Mater.* **2019**, *4*, 4.
[3] C. Ortiz-Cervantes, P. Carmona-Monroy, D. Solis-Ibarra, *ChemSusChem* **2019**, *12*, 1560.
[4] H. Ren, S. Yu, L. Chao, Y. Xia, Y. Sun, S. Zuo, F. Li, T. Niu, Y. Yang, H. Ju, B. Li, H. Du, X. Gao, J. Zhang, J. Wang, L. Zhang, Y. Chen, W. Huang, *Nat. Photonics* **2020**, *14*, 154.
[5] D. T. Gangadharan, D. Ma, *Energy Environ. Sci.* **2019**, *12*, 2860.
[6] M. C. Gélvez-Rueda, E. M. Hutter, D. H. Cao, N. Renaud, C. C. Stoumpos, J. T. Hupp, T. J. Savenije, M. G. Kanatzidis, F. C. Grozema, *J. Phys. Chem. C* **2017**, *121*, 26566.
[7] M. C. Gélvez-Rueda, P. Ahlawat, L. Merten, F. Jahanbakhshi, M. Mladenović, A. Hinderhofer, M. I. Dar, Y. Li, A. Dučinskas,

B. Carlsen, W. Tress, A. Ummadisingu, S. M. Zakeeruddin, F. Schreiber, A. Hagfeldt, U. Rothlisberger, F. C. Grozema, J. V. Milić, M. Graetzel, *Adv. Funct. Mater.* **2020**, *30*, 2003428.
[8] Y. Qin, H. Zhong, J. J. Intemann, S. Leng, M. Cui, C. Qin, M. Xiong, F. Liu, A. K. -Y. Jen, K. Yao, *Adv. Energy Mater.* **2020**, *10*, 1904050.
[9] J. Dong, S. Shao, S. Kahmann, A. J. Rommens, D. Hermida-Merino, G. H. t. Brink, M. A. Loi, G. Portale, *Adv. Funct. Mater.* **2020**, *30*, 2001294.
[10] C. M. M. Soe, G. P. Nagabhushana, R. Shivaramaiah, H. Tsai, W. Nie, J.-C. Blancon, F. Melkonyan, D. H. Cao, B. Traoré, L. Pedesseau, M. Kepenekian, C. Katan, J. Even, T. J. Marks, A. Navrotsky, A. D. Mohite, C. C. Stoumpos, M. G. Kanatzidis, *Proc. Natl. Acad. Sci. USA* **2019**, *116*, 58.
[11] J.-W. Lee, H.-S. Kim, N.-G. Park, *Acc. Chem. Res.* **2016**, *49*, 311.
[12] B. Li, D. Binks, G. Cao, J. Tian, *Small* **2019**, *15*, 1903613.
[13] J.-W. Lee, Z. Dai, C. Lee, H. M. Lee, T.-H. Han, N. De Marco, O. Lin, C. S. Choi, B. Dunn, J. Koh, D. Di Carlo, J. H. Ko, H. D. Maynard, Y. Yang, *J. Am. Chem. Soc.* **2018**, *140*, 6317.
[14] S. Shao, H. Duim, Q. Wang, B. Xu, J. Dong, S. Adjokatse, G. R. Blake, L. Protesescu, G. Portale, J. Hou, M. Saba, M. A. Loi, *ACS Energy Lett.* **2020**, *5*, 39.
[15] N. Liu, P. Liu, H. Ren, H. Xie, N. Zhou, Y. Gao, Y. Li, H. Zhou, Y. Bai, Q. Chen, *ACS Appl. Mater. Interfaces* **2020**, *12*, 3127.
[16] Y. Xu, M. Wang, Y. Lei, Z. Ci, Z. Jin, *Adv. Energy Mater.* **2020**, *10*, 2002558.
[17] A. Z. Chen, M. Shiu, J. H. Ma, M. R. Alpert, D. Zhang, B. J. Foley, D. M. Smilgies, S. H. Lee, J. J. Choi, *Nat. Commun.* **2018**, *9*, 1336.
[18] J. M. Hoffman, J. Strzalka, N. C. Flanders, I. Hadar, S. A. Cuthriell, Q. Zhang, R. D. Schaller, W. R. Dichtel, L. X. Chen, M. G. Kanatzidis, *Adv. Mater.* **2020**, *32*, 2002812.
[19] C. M. M. Soe, W. Nie, C. C. Stoumpos, H. Tsai, J. C. Blancon, F. Liu, J. Even, T. J. Marks, A. D. Mohite, M. G. Kanatzidis, *Adv. Energy Mater.* **2018**, *8*, 1700979.
[20] R. Quintero-Bermudez, A. Gold-Parker, A. H. Proppe, R. Munir, Z. Yang, S. O. Kelley, A. Amassian, M. F. Toney, E. H. Sargent, *Nat. Mater.* **2018**, *17*, 900.
[21] A. Z. Chen, M. Shiu, X. Deng, M. Mahmoud, D. Zhang, B. J. Foley, S.-H. Lee, G. Giri, J. J. Choi, *Chem. Mater.* **2019**, *31*, 1336.
[22] C. J. Dahlman, R. A. DeCrescent, N. R. Venkatesan, R. M. Kennard, G. Wu, M. A. Everest, J. A. Schuller, M. L. Chabinyc, *Chem. Mater.* **2019**, *31*, 5832.
[23] Y. Hu, L. M. Spies, D. Alonso-Álvarez, P. Mocherla, H. Jones, J. Hanisch, T. Bein, P. R. F. Barnes, P. Docampo, *J. Mater. Chem. A* **2018**, *6*, 22215.
[24] P. Mao, J. Zhuang, Y. Wei, N. Chen, Y. Luan, J. Wang, *Sol. RRL* **2019**, *3*, 1800357.
[25] P. Cheng, Z. Xu, J. Li, Y. Liu, Y. Fan, L. Yu, D.-M. Smilgies, C. Müller, K. Zhao, S. F. Liu, *ACS Energy Lett.* **2018**, *3*, 1975.
[26] X. Li, J. M. Hoffman, M. G. Kanatzidis, *Chem. Rev.* **2021**, *121*, 2230.
[27] J. Liu, J. Leng, K. Wu, J. Zhang, S. Jin, *J. Am. Chem. Soc.* **2017**, *139*, 1432.
[28] P. Cheng, P. Wang, Z. Xu, X. Jia, Q. Wei, N. Yuan, J. Ding, R. Li, G. Zhao, Y. Cheng, K. Zhao, S. F. Liu, *ACS Energy Lett.* **2019**, *4*, 1830.
[29] C. C. Stoumpos, D. H. Cao, D. J. Clark, J. Young, J. M. Rondinelli, J. I. Jang, J. T. Hupp, M. G. Kanatzidis, *Chem. Mater.* **2016**, *28*, 2852.
[30] R. Yang, R. Li, Y. Cao, Y. Wei, Y. Miao, W. L. Tan, X. Jiao, H. Chen, L. Zhang, Q. Chen, H. Zhang, W. Zou, Y. Wang, M. Yang, C. Yi, N. Wang, F. Gao, C. R. McNeill, T. Qin, J. Wang, W. Huang, *Adv. Mater.* **2018**, *30*, 1804771.
[31] W. L. Tan, Y.-B. Cheng, C. R. McNeill, *J. Mater. Chem. A* **2020**, *8*, 12790.
[32] J. Song, G. Zhou, W. Chen, Q. Zhang, J. Ali, Q. Hu, J. Wang, C. Wang, W. Feng, A. B. Djurišić, H. Zhu, Y. Zhang, T. Russell, F. Liu, *Adv. Mater.* **2020**, *32*, 2002784.
[33] H. Tsai, W. Nie, J.-C. Blancon, C. C. Stoumpos, R. Asadpour, B. Harutyunyan, A. J. Neukirch, R. Verduzco, J. J. Crochet, S. Tretiak, L. Pedesseau, J. Even, M. A. Alam, G. Gupta, J. Lou, P. M. Ajayan, M. J. Bedzyk, M. G. Kanatzidis, A. D. Mohite, *Nature* **2016**, *536*, 312.
[34] J. Shi, Y. Gao, X. Gao, Y. Zhang, J. Zhang, X. Jing, M. Shao, *Adv. Mater.* **2019**, *31*, 1901673.
[35] X. Li, G. Wu, M. Wang, B. Yu, J. Zhou, B. Wang, X. Zhang, H. Xia, S. Yue, K. Wang, C. Zhang, J. Zhang, H. Zhou, Y. Zhang, *Adv. Energy Mater.* **2020**, *10*, 2001832.
[36] C. Zuo, A. D. Scully, W. L. Tan, F. Zheng, K. P. Ghiggino, D. Vak, H. Weerasinghe, C. R. McNeill, D. Angmo, A. S. R. Chesman, M. Gao, *Commun. Mater.* **2020**, *1*, 33.
[37] L. Li, Y. Chen, Z. Liu, Q. Chen, X. Wang, H. Zhou, *Adv. Mater.* **2016**, *28*, 9862.
[38] Y. Han, S. Park, J. Wang, S. Jariwala, K. Lee, C. G. Bischak, S. Kim, J. Hong, S. Kim, M. J. Lee, D. S. Ginger, I. Hwang, *Adv. Mater. Interfaces* **2020**, *7*, 2070017.
[39] G. Wu, T. Yang, X. Li, N. Ahmad, X. Zhang, S. Yue, J. Zhou, Y. Li, H. Wang, X. Shi, S. Liu, K. Zhao, H. Zhou, Y. Zhang, *Matter* **2021**, *4*, 582.